Experimental Investigation of Flow About a Strut-Endwall Configuration

P. S. Chang*
Aerospace Corporation, El Segundo, California 90245
and
F. B. Gessner†
University of Washington, Seattle, Washington 98195

An experimental study was conducted to investigate incompressible flow about a strut-endwall configuration positioned within a constant area duct. The endwall boundary layer was tripped, but natural transition occurred on the strut surface. The results indicate that a secondary vortex is formed that coexists with the horseshoe vortex generated by endwall flow separation upstream of the strut leading edge. Both vortices are similar in strength downstream of the strut trailing edge, and both distort the primary flow and local turbulence structure in the wake-endwall region. The level of distortion is demonstrated by means of axial mean velocity contours, turbulence kinetic-energy contours, and Reynolds shear stress contours measured in the cross plane at two streamwise locations. Analysis of the results shows that conventional eddy viscosity and $k-\epsilon$ transport equation models are not wholly adequate for predicting this flow situation.

Nomenclature

a,b	= relative positions of sensor, Fig. 2
C	= law-of-the-wall constant, 5.2
C_p	= pressure coefficient, $(p - p_i)/[(1/2)\rho U_b^2]$
c	= strut chord
d	= support diameter, Fig. 2
h	= half-height of upper duct, Fig. 1
k	= turbulence kinetic energy
P	= turbulence kinetic energy production rate
p	= static pressure
p_t	= total pressure
U	= x direction mean velocity component
$U+$	= normalized value of U, yU_τ/v
$U\tau$	= friction velocity, $\sqrt{\tau_w/\rho}$
$\overline{u^2}$, $\overline{v^2}$, $\overline{w^2}$	= Reynolds normal stress components
$\overline{uv}$, $\overline{uw}$, $\overline{vw}$	= Reynolds shear stress components
V, W	= y and z direction mean velocity components
V_r	= resultant transverse mean component, $(V^2 + W^2)^{1/2}$
x,y,z	= Cartesian coordinates, Fig. 1
$y+$	= normalized value of y, yU_τ/v
α	= flow angle in x,y plane, $\tan^{-1}(V/U)$
β	= generalized Falkner-Skan parameter
δ	= boundary-layer thickness
ϵ	= turbulence kinetic energy dissipation rate
κ	= von Kármán's constant, 0.4
ν	= kinematic viscosity
ρ	= density
τ_w	= wall shear stress

Subscripts

b	= bulk flow
c	= core flow
i	= inlet flow
s	= strut surface

Received April 26, 1990; presented as Paper 90-1541 at the 21st AIAA Fluid Dynamics, Plasmadynamics, and Lasers Conference, Seattle, WA, June 18-20, 1990; revision received Oct. 1, 1990; accepted for publication Oct. 5, 1990.

*Technical Staff Member, Spacecraft Thermal Department, MS M4/908.

†Professor, Department of Mechanical Engineering. Member AIAA.

Introduction

In flow about a typical strut-endwall configuration, spanwise vorticity in the upstream boundary layer is converted into streamwise vorticity by virtue of horseshoe formation about the strut. The counter-rotating vortices that exist on either side of the strut distort the primary flow and the local turbulence structure, both in the vicinity of the intersection and in the wake-endwall region downstream. Recent work in this area by Devenport and Simpson[1-3] has shown that flow in the vicinity of the nose of a typical wing-body type juncture is unsteady in the mean, even when the upstream flow is steady. More specifically, the results of their most recent study[3] show that flow in the plane of symmetry immediately upstream of a 3:2 elliptical nose is characterized by large-scale, low-frequency unsteadiness. This unsteadiness is bimodal in nature, with streamwise mean velocities near the wall alternating between large negative values (the backflow mode) and near-zero values (the zero-flow mode). When the zero-flow mode is present (approximately 20–30% of the time), a relatively weak counter-rotating recirculation pattern exists near the wall upstream of the primary recirculation pattern. This behavior differs markedly from the results of surface oil flow visualization studies, which appear to indicate the presence of four recirculation zones in this region for a semicircular nose configuration.[4-6] The time-dependent recirculation patterns observed by Devenport and Simpson also differ from those obtained by continuous, time-averaged measurements, which indicate the presence only of a single dominant vortex in the plane of symmetry upstream of a semicircular nose, with the possible presence of additional vortices near the wall.[6,7]

In as yet unpublished work, the same type of unsteadiness observed in the plane of symmetry upstream of the 3:2 elliptical nose employed in Refs. 1-3 has also been observed immediately upstream of the nose of a Rankine half-body.[3] Other data presented by Devenport and Simpson[8] show that time-dependent flow behavior observed in the nose region can extend downstream to the point of maximum airfoil thickness. The degree of unsteadiness is probably a relatively strong function of nose bluntness. The time-dependent separation and reattachment processes that occur in the vicinity at the nose must be modeled accurately if all features of the flow are to be predicted correctly. From a practical point of view, however, steady-state forms of the Reynolds-averaged equations will probably continue to be used as a basis for analysis in the

near future, so that experimental results that focus on observed time-averaged behavior are of interest for purposes of comparison. Menna and Pierce[9] and Pierce and Harsh,[10] for example, have recently generated comprehensive mean flow and Reynolds stress data sets in the vicinity of a wing-body juncture that are suitable for comparison with numerical predictions. Their airfoil configuration had a relatively large (1:2.4) thickness-to-chord ratio and consisted of a semicircular nose connected to a linearly tapered tail. For this configuration, local flow separation was observed to occur near the trailing edge, so that prediction of their particular flow situation presents a challenging task. Other data sets in the vicinity of the intersection have been generated for wholly attached flow over the airfoil or strut. These studies include those for which the airfoil configuration corresponded to a Rankine halfbody[11] or was of constant width downstream of an elliptical nose.[12-14] Data have also been obtained for juncture flows using airfoils formed by a semicircular nose connected to either a linearly tapered[15] or streamlined tail[6] and airfoils with wedge-elliptic leading and trailing edges.[5]

In reference to flow in the wake-endwall region downstream of the trailing edge, mean velocity and Reynolds stress data are available for a relatively thin (1:50 thickness-to-chord ratio) airfoil with a rounded leading edge and wedge-shaped tail, mounted on a flat plate having a rounded leading edge coincident with the airfoil leading edge.[16] Under these circumstances, corner-generated vortices dominate the flow, inasmuch as no horseshoe vortex is generated for a coincident leading-edge condition. Some data in the wake-endwall region are also now available for a Joukowsky-type airfoil mounted on a flat plate at a 30-deg angle of attack.[17,18] One interesting feature of this flow is the presence of a tornado-type, spanwise vortex downstream of the trailing edge that rises from the endwall surface before it bends downstream and becomes a longitudinal (streamwise) vortex. This reorientation of vorticity in the flow distorts not only flow patterns in the cross plane, but also static pressure and skin friction coefficient distributions on the endwall.

The present study was initiated to investigate flow on the downstream side of a typical wing-body juncture and in the wake-endwall region downstream. With the exception of the limited results presented in Refs. 16-18, there is relatively little information available on the decay of the horseshoe vortex in this region and its attendant influence on the local flow structure. In many of the aforementioned studies, local flow behavior in the vicinity of a wing-body juncture was examined for zero pressure gradient flow conditions. In the present study, a wing-body configuration was positioned within a constant area duct to induce a favorable pressure gradient flow more representative of that which exists within constant area, axisymmetric ducts having struts that act as supports between the cowl and centerbody. This type of wing-body juncture is more properly termed a strut-endwall intersection, and this terminology shall be used in subsequent discussion. Natural transition was allowed to occur on the strut surface, but the endwall boundary layer was tripped upstream. This operating condition existed in almost all of the aforementioned studies, with the exception of the studies by Devenport and Simpson[1-3] and Devenport et al.,[19] for which the wing boundary layer was tripped just upstream of maximum airfoil thickness.

Experimental Apparatus and Procedure

Basic Flow Facility

The basic flow facility is an open-circuit wind tunnel with a test section consisting of a Formica-lined square duct (25.4 cm × 25.4 cm) preceded by a square contraction, as shown in Fig. 1. Atmospheric air enters a plenum chamber that is located immediately upstream of the contraction and is fitted with filters, screens, and a honeycomb. This combination of devices yields an axial flow at the duct inlet that is spanwise uniform to within 0.5% over 98% of the centered duct width. The streamwise turbulence level in the core flow at this location is less than 0.2%. The strut-endwall configuration located within the duct consists of two NACA 0012 airfoils positioned on either side of a horizontal splitter plate centered within the duct. For reference purposes, an x,y,z coordinate system is defined relative to the strut leading edge as shown in Fig. 1.

A splitter plate was used in the present study in lieu of having the strut extend across the height of the duct to ensure a spanwise uniform flow upstream of the strut-endwall intersection. Preliminary data taken at the duct inlet indicated that "wrinkles" were present in the centered portion of isovelocity contours measured near the roof and the floor of the duct, probably as a result of streamline convergence within the contraction.[20] Under these conditions, flow immediately upstream of any strut in contact with the roof and floor of the duct might not be spanwise uniform if the development length of the flow were not sufficient to smooth out these nonuniformities. Rather than risk this behavior, two struts were positioned on either side of a splitter plate in the present study.

The struts and splitter plate were made of aluminum, and all surfaces exposed to the flow were polished. A boundary-layer trip consisting of a 2-cm width strip of no. 36 grit sandpaper was installed around the periphery of the upper and lower ducts (formed by the addition of a splitter plate) just downstream of the duct inlet (at $x/c = -3.7$; refer to Fig. 1). The wedge-shaped leading edge of the splitter plate was positioned at a

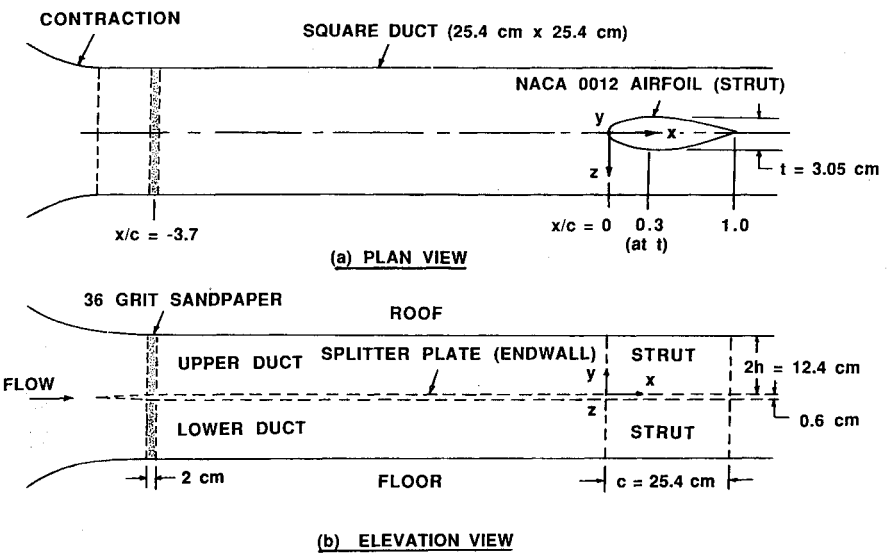

Fig. 1 Strut-endwall configuration inside square duct.

streamwise location that induced essentially the same boundary-layer growth on the roof and endwall surfaces of the upper duct. For the configuration shown in Fig. 1 and an operating inlet (bulk) velocity of 15.8 m/s, the boundary-layer thickness on the roof and endwall upstream of the strut leading edge (at $x/c = -2.0$, $z/c = 0$) was 1.52 cm or one-half of the maximum thickness of the strut (3.05 cm). Probes were positioned at y,z locations in the upper duct to within ± 0.025 mm by means of dial gauges and a two-component traversing mechanism that was mounted on the roof of the duct and could be positioned at different streamwise locations. All flowfield data were taken with hole-free strut and endwall sections installed within the duct. These configurations were replaced by duplicate configurations having arrays of 0.5 mm diam static pressure taps to obtain surface pressure distributions.

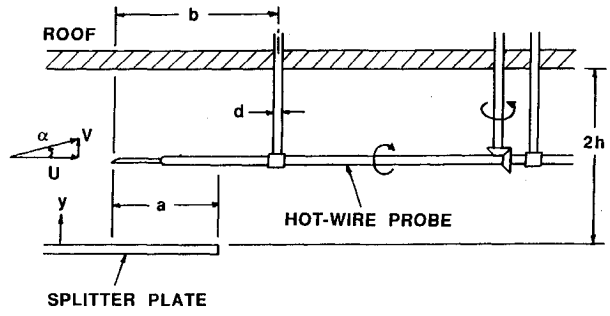

Fig. 2 Hot-wire probe orientation relative to trailing edge of splitter plate.

Pressure Probe Instrumentation

Flattened boundary-layer probes with outer tip dimensions 0.3 mm × 0.6 mm were used to measure total pressure and velocity pressure (when referenced to a wall tap) at points in the near-wall region whenever the local crossflow component was less than 2% of the axial component. Two pitot-static tubes with a tip diameter of 1.5 mm were used to measure local mean velocity in the cross plane and at various streamwise locations in the core flow. One of these probes had a tip whose pivot point coincided with the longitudinal (rotation) axis of the probe body, so that the tip could be aligned with the local mean flow direction in the yaw plane before data were taken. Two different diameter Preston tubes were used to measure axial wall shear stress distributions on the endwall in the undisturbed region upstream of the strut-endwall intersection (2.1 mm and 3.0 mm o.d. probes) and in the wake-endwall region at streamwise locations where skewness levels near the endwall were less than 3 deg (3.0 mm and 4.5 mm o.d. probes). The data were reduced by means of tabulated Preston tube calibration data presented by Head and Vasanta Ram.[21] Friction velocity values calculated from data taken with two different diameter probes at a given location differed by less than 1.5% at all locations. This method of evaluating the friction velocity presumes that axial mean velocity distributions near the endwall follow local law-of-the-wall behavior, an assumption that will be justified later. Differential pressures were measured by means of a Barocel pressure sensor, Type 571D-10T-1C2-VI, operated in conjunction with a Barocel Type 1174 electronic manometer. To facilitate static pressure measurements on the strut and endwall surfaces, two 48-channel Scanivalve units (Model 48J9) were used in conjunction with the Barocel pressure transducer system.

Hot-Wire Instrumentation

Mean velocity and Reynolds stress measurements were made by means of the single-wire rotation technique described by Gessner and Arterberry.[22] This method is based on the sequential use of inclined and normal wire probes whose bodies are aligned with the axial flow direction, as shown in Fig. 2. The technique can be used to determine the three mean velocity components and all six components of the Reynolds stress tensor in relatively low intensity flows that are arbitrarily skewed in pitch and yaw by as much as 20 deg relative to the probe body (an upper limit not exceeded in the present investigation). The response equations are fourth-order accurate relative to the crossflow components V and W, but are first-order accurate relative to the turbulent fluctuations, so that the mean-response equations are uncoupled from the turbulence response equations. The three mean velocity components were determined from data obtained by rotating the inclined wire probe about the x axis to four positions, 90 deg apart and aligned with y,z coordinates. The six Reynolds stress components were determined by coupling normal wire data with data obtained by rotating the inclined wire probe to eight positions whose pattern depended on the local skewness level in the flow. In regions of the flow where the local skewness level did not exceed 3 deg, the inclined wire probe was rotated in 45-deg increments relative to laboratory (x,y,z) coordinates, and the simplified response equations given by Po[23] were used to calculate the Reynolds stresses.

The sensors of the normal and inclined wire probes were made from 0.0038 mm (3.8 μ) diam tungsten wire. Each sensor was mounted between tapered probe fingers, 3 mm apart, and had a centered active length of 0.7 ± 0.025 mm. The probes were energized by means of a TSI Model 1010 constant temperature anemometer. The mean output voltage from the anemometer was read on a DISA Type 55D31 digital voltmeter, and the mean square of the fluctuating voltage was read on a second DISA Type 55D31 digital voltmeter connected to a TSI Model 1060 rms voltmeter. The inclined wire probe was calibrated in fully developed pipe flow to prescribe a value for the yaw sensitivity factor (0.15) in the hot-wire response equations. The pitch sensitivity factor was specified as 0.9 on the basis of calibration data obtained previously by Arterberry.[24] Both the normal and inclined wire probes were calibrated in the potential core of a free jet to prescribe calibration slope and intercept values in the response equations. The cold resistance of each wire was also measured before and during each run to check for wire drift. If the values differed by more than $\pm$ 0.02 ohm (relative to a nominal cold resistance of 4.0 to 4.2 ohms), the wire was removed from the duct and recalibrated. Throughout the present series of experiments, wire calibration slope and intercept values differed by less than 2% between successive calibrations. More complete details of the probe configurations, measurement techniques, and data reduction procedures are given by Chang.[25]

Uncertainty Estimates

Uncertainty estimates were made for variables measured at the trailing edge of the strut ($x/c = 1.0$) where peak turbulence levels were found to exist. The estimated uncertainty in pressure-probe-based values of U/U_b at this location is less than 1% over the entire cross section where data were taken ($0 < y/h \leq 1.0$, $0 < z/h \leq 1.0$). The estimated uncertainty in pressure coefficient (C_p) values measured in the core flow and on the strut and endwall surfaces is 2.3%. To calculate uncertainties in the hot-wire based variables, uncertainty levels were assigned to the wire inclination angle (nominally 45 deg), to calibration slope and intercept values, and to mean and mean-square fluctuating voltages measured at various points in the flow. In the region distant from the endwall and strut surfaces, where peak uncertainty levels exist ($0.6 \leq y/h \leq 1.0$, $0.6 \leq z/h \leq 1.0$), the estimated uncertainty in measured values of $\bar{U}/U_b$, $\bar{V}/U_b$, and $\bar{W}/U_b$ is 0.6, 3.0, and 3.0%, respectively. The uncertainty in the Reynolds normal stress components $\overline{u^2}/U_b^2$, $\overline{v^2}/U_b^2$ and $\overline{w^2}/U_b^2$ was estimated as 3.6, 5.9, and 5.9%, respectively, with a corresponding uncertainty of 9.1% for the turbulence kinetic energy. The uncertainty in the Reynolds shear stress components $\overline{uv}/U_b^2$, $\overline{uw}/U_b^2$, and $\overline{vw}/U_b^2$ was estimated as 4.7, 4.7, and 6.4%, respectively, for this region. In regions of the flow closer to the endwall and strut surfaces, the uncertainty levels are lower than the aforementioned

values. This is also the case for data obtained at other streamwise locations, where peak turbulence intensities were less than those observed near the strut trailing edge.

Results and Discussion

Preliminary Measurements

To examine local flow symmetry, total pressure contours were measured in the cross plane at a streamwise location corresponding to maximum strut thickness ($x/c = 0.3$) and in the wake-endwall region downstream ($x/c = 3.3$). The results are shown in Fig. 3, where points *A, B, C,* and *D* are symmetrically located with respect to the horizontal and vertical midplanes of the duct, $y/h = 1.0$ and $z/h = 0$, respectively. From the figure it can be seen that the flow is locally symmetric with respect to points *C* and *D*, but that some asymmetry exists in the vicinity of points *A* and *B* at both streamwise locations. This asymmetry is a direct result of the spanwise nonuniform flow at the duct inlet induced by streamline convergence effects in the contraction upstream, as noted earlier, and demonstrates the advantage of using a wing splitter plate in the present study. On the basis of the results shown in Fig. 3, a measurement quadrant was selected, defined as shown in Fig. 3, where detailed measurements of flow in the cross plane were made, both in the vicinity of the strut-endwall intersection (at $x/c = 0.3$ and 1.0) and in the wake-endwall region downstream (at $x/c = 1.8$ and 3.3). The data were taken at points on a 12 × 13 grid within the quadrant, and interpolation was applied to construct isocontours of the variables. Initial data were taken upstream of the intersection to examine spanwise uniformity of the flow and to provide data for matching purposes with numerical predictions. Axial mean velocity distributions measured at three spanwise locations ($z/h = -1.0$, 0, and 1.0) at $x/c = -2.0$ were essentially coincident and in excellent agreement with the law of the wall. Tabulated velocity values in terms of both conventional and law-of-the-wall coordinates are given by Chang.[25]

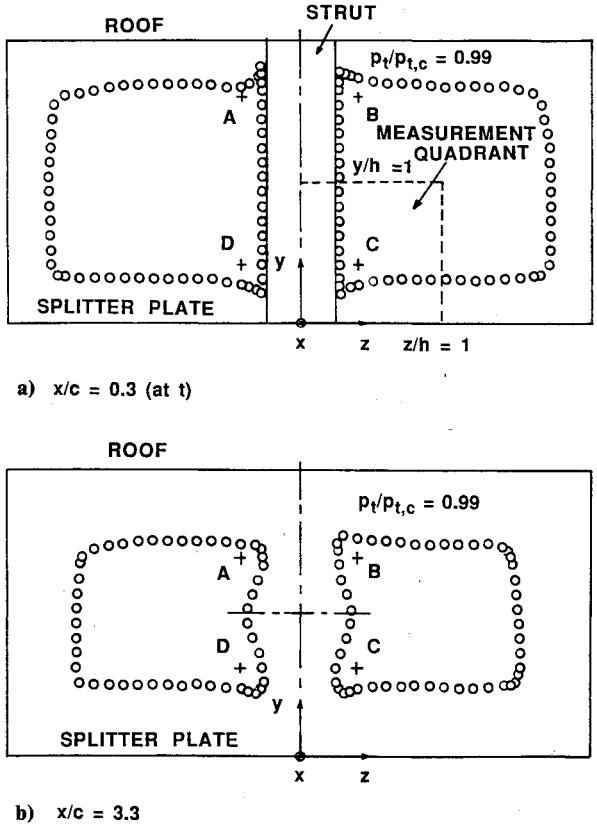

Fig. 3 Total pressure contours at two streamwise locations in the upper duct.

In making hot-wire measurements with forward-facing probes as shown in Fig. 2, it was recognized that flow in the vicinity of the sensor would be sensitive to blockage effects induced by the forward-most probe support passing through the roof and by downwash effects induced by streamline convergence downstream of the trailing edge of the splitter plate. To investigate these effects, the local flow angle in the *x,y* plane (α), defined as shown in Fig. 2, was measured at points along the midplane traverse $y/h = 1.0$, a line along which α should be identically zero on the basis of symmetry considerations (refer to Fig. 3). Initial data taken with the inclined wire probe positioned 3.8 cm upstream of the trailing edge ($a/h = 0.6$) and 7.6 cm upstream of the first support ($b/d = 12$) yielded values for α that ranged between -0.6 and -0.74 deg over the transverse interval $0 \leq z/h \leq 1.0$. Inasmuch as downwash angles of this magnitude were considered unacceptable, the traversing mechanism that held the probe was repositioned, and the sensor was relocated further upstream of the trailing edge to a location for which $a/h = 2.7$ and $b/d = 30$. Under these conditions, measured values of α ranged between -0.04 and $+0.08$ deg over the same transverse interval, which indicated that blockage and downwash effects on the data had been essentially eliminated. These relative positions ($a/h =$

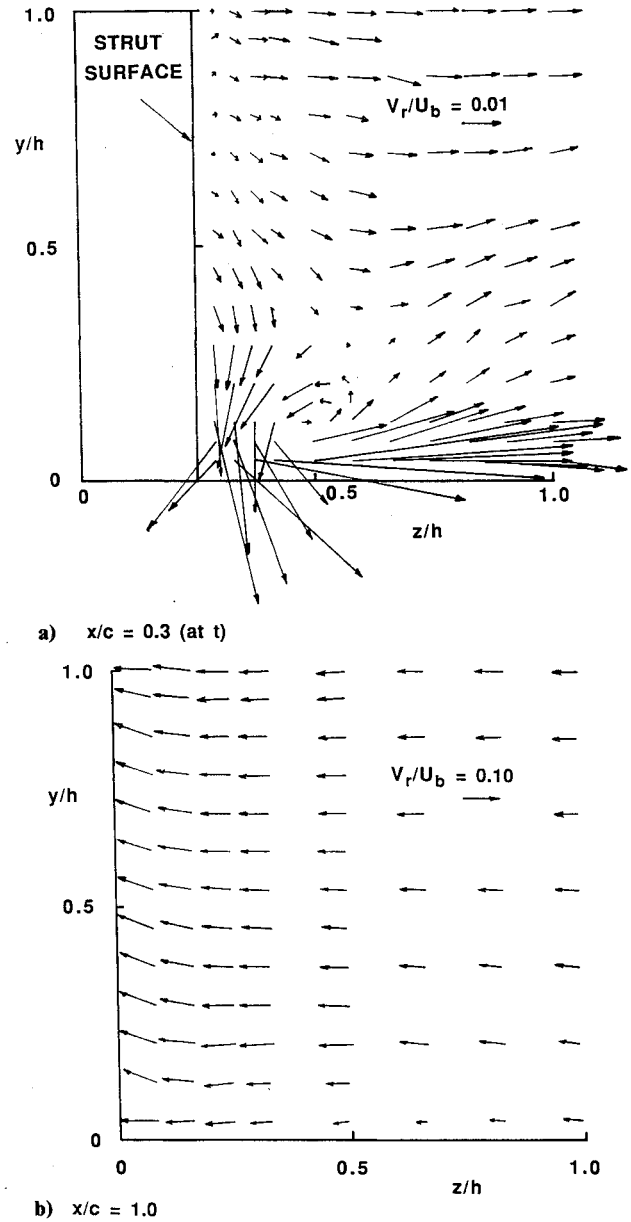

Fig. 4 Crossflow velocity vectors in the vicinity of the intersection.

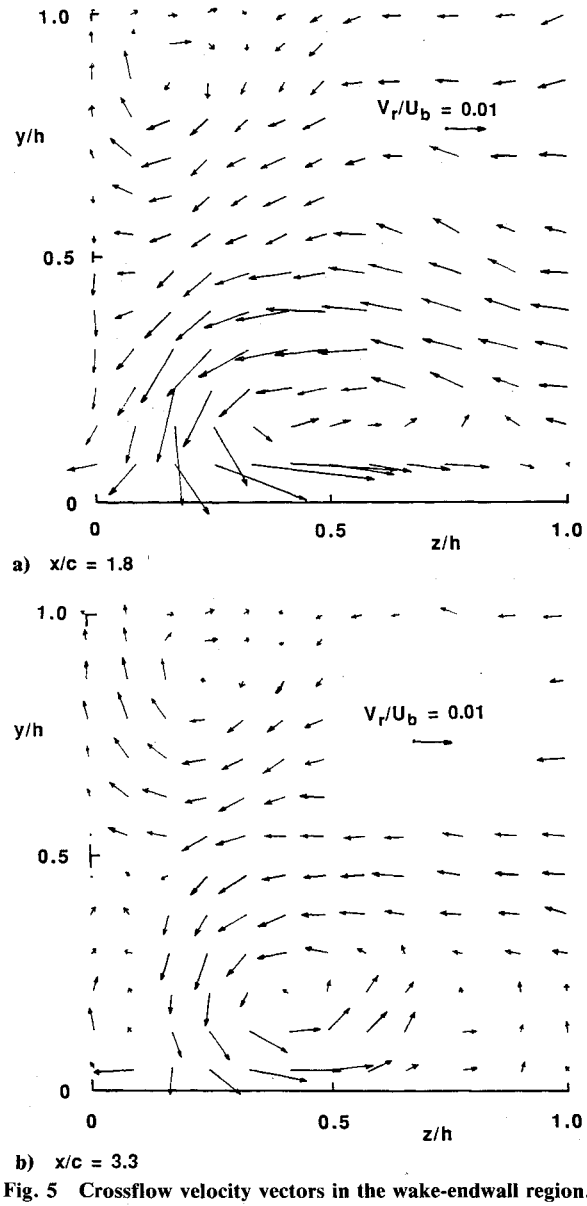

Fig. 5 Crossflow velocity vectors in the wake-endwall region.

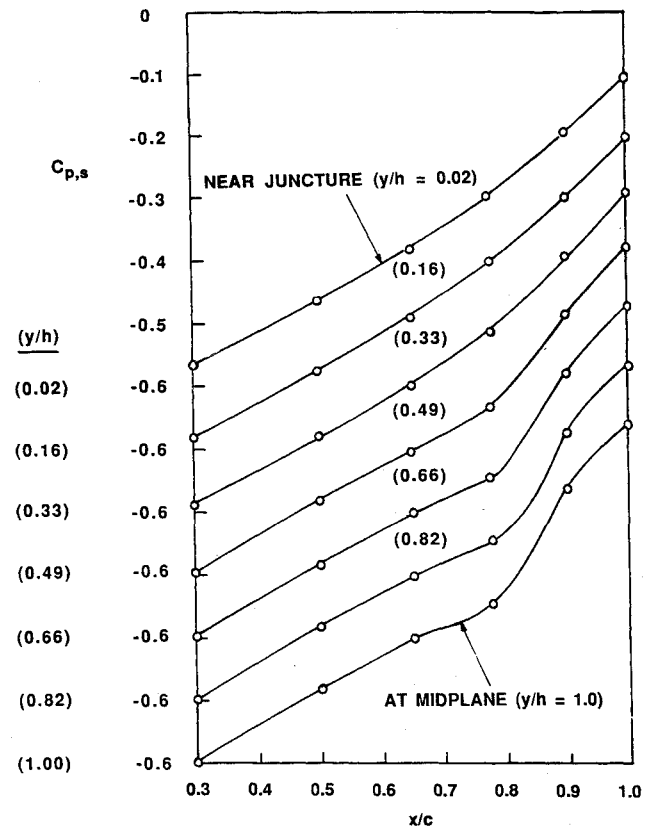

Fig. 6 Pressure coefficient distributions on the strut surface.

2.7 and b/d = 30) were maintained when hot-wire data were taken at the four streamwise locations (x/c = 0.3, 1.0, 1.8, and 3.3) by successively extending the length of the splitter plate.

Mean Flow Results

The crossflow velocity patterns measured at two streamwise locations along the strut are shown in Fig. 4. In reference to Fig. 4a, it can be seen that there is a weak counterclockwise vortex in the vicinity of the intersection at maximum strut thickness (x/c = 0.3) and a relatively strong, outwardly directed flow near the endwall. The overall pattern is qualitatively similar to patterns that have been measured in the vicinity of a wing-body juncture just downstream of an elliptic nose connected to a constant thickness body.[26,27] The presence of a corner-generated vortex was not observed in the present study, although previous surface flow visualization studies have shown that it exists.[5,13,28] The strength of the horseshoe vortex in Fig. 4a is somewhat weaker than that observed just downstream of a semicircular nose,[30] probably because a more streamlined nose configuration was used in the present study. At the trailing edge (x/c = 1.0), Fig. 4b shows that the presence of this vortex is masked by a strong transverse flow in the $-z$ direction induced by strut convergence between x/c = 0.3 and 1.0. (Note the 10:1 increase in the velocity scale in this figure in comparison to that shown in Fig. 4a.) Downstream in the wake region at x/c = 1.8, Fig. 5a shows that a second, clockwise vortex now appears in addition to the counterclockwise horseshoe vortex. Further measurements at this location confirmed the existence of a mirror-image vortex directly above the secondary vortex. A comparison of the results in Figs. 5a and 5b shows that the strength of the horseshoe vortex diminishes between x/c = 1.8 and 3.3, while the secondary vortex maintains its strength between these two locations, presumably because there is no adjacent surface to inhibit its motion.

The secondary vortex that exists in the wake-endwall region does not appear to be directly induced by the horseshoe vortex on the basis of the following considerations. Figure 4b shows that there is a relatively strong upwash flow near the trailing edge of the strut along its entire span. The direction of this flow is opposite to the downwash flow observed by Harsh and Pierce[29] at the trailing edge of their wing-body configuration. Bradshaw[30] attributes this downwash flow to the sudden removal of the opposing force exerted by the spanwise shear stress component on the strut surface as the flow proceeds past the trailing edge. If this effect were dominant in the present study, then a downwash flow should appear in the vicinity of the trailing edge of the present strut-endwall configuration, but as Fig. 4b indicates, this is clearly not the case. Indeed, the appearance of an upwash flow near the trailing edge is counter to what one would expect from direct inducement by a counterclockwise horseshoe vortex.

Instead, the observed upwash flow probably occurs because of a lateral flow in the $-z$ direction near the endwall surface induced by transverse pressure gradients acting on the curved flow between the convex strut surface and duct side wall. Inasmuch as y/h = 1.0 is a plane of symmetry, upwash flow near the strut surface must turn outward in the vicinity of this plane. Because the flow is bounded by the duct side wall at z/h = 2.0 (refer to Fig. 3), the transverse flow must turn downward before the side wall is reached. The horseshoe vortex, through the action of viscosity, then apparently causes this

transverse flow to be directed toward the strut surface, which completes the cycle and leads to the formation of a closed vortical flow pattern. This same sequence of events would occur if the duct side wall were replaced by another strut to simulate a stator cascade. The strength of the secondary vortex that is generated by this process must be a function of the spacing between the parallel endwalls that bound the strut, inasmuch as this type of vortex has not been observed in previous studies of unconfined, wing-body juncture flows.

The flow appears to be further complicated by the presence of a separation bubble on the strut. Figure 6 shows pressure coefficient distributions measured on the strut surface between maximum strut thickness ($x/c = 0.3$) and the trailing edge ($x/c = 1.0$). In the near vicinity of the juncture (e.g., at $y/h = 0.02$ and 0.16), the distributions increase monotonically with no anomalous behavior. In the vicinity of the midplane, however, (e.g., at $y/h = 0.82$ and 1.0), pressure coefficient values increase at a slower rate between $x/c = 0.65$ and 0.77 and then increase more rapidly between $x/c = 0.77$ and 0.9. This behavior is compatible with what one would anticipate from streamline convergence and divergence effects induced by a separation bubble in this region. The bubble itself appears to be basically unsteady, inasmuch as Reynolds stress distributions measured in the near vicinity of the bubble, specifically at the trailing edge along the midplane traverse $z/h = 1.0$, are all elevated in comparison to distributions measured by Klebanoff[31] for zero pressure gradient, flat-plate flow. These elevated levels are too high to be the result of streamwise adverse pressure gradient effects alone in the flow. Additional measurements along the same traverse ($z/h = 1.0$) at $x/c = 3.3$ in the wake-endwall region, where the streamwise pressure gradient was weakly favorable, yielded Reynolds stress values that agreed well with Klebanoff's results. These comparisons indicated that the hot-wire anemometer system was performing properly and that the elevated stress levels measured at the trailing edge are a real effect.

Axial mean velocity contours measured at the four streamwise locations are shown in Figs. 7 and 8. The pressure probe and hot-wire probe results are in generally good agreement at all streamwise locations. In reference to Fig. 7a, no contours are shown adjacent to the strut surface, inasmuch as the boundary layer thickness on this surface at $x/c = 0.3$, excluding the immediate vicinity of the intersection, was less than 2 mm ($\Delta z/h < 0.013$), and no flowfield data were taken in this region. A comparison of Figs. 4b and 7b shows that isovelocity contours measured near the strut surface at the trailing edge are essentially parallel to this surface, even though there is a relatively strong upward crossflow in this region. Inasmuch as the isovelocity contours are not distorted near the

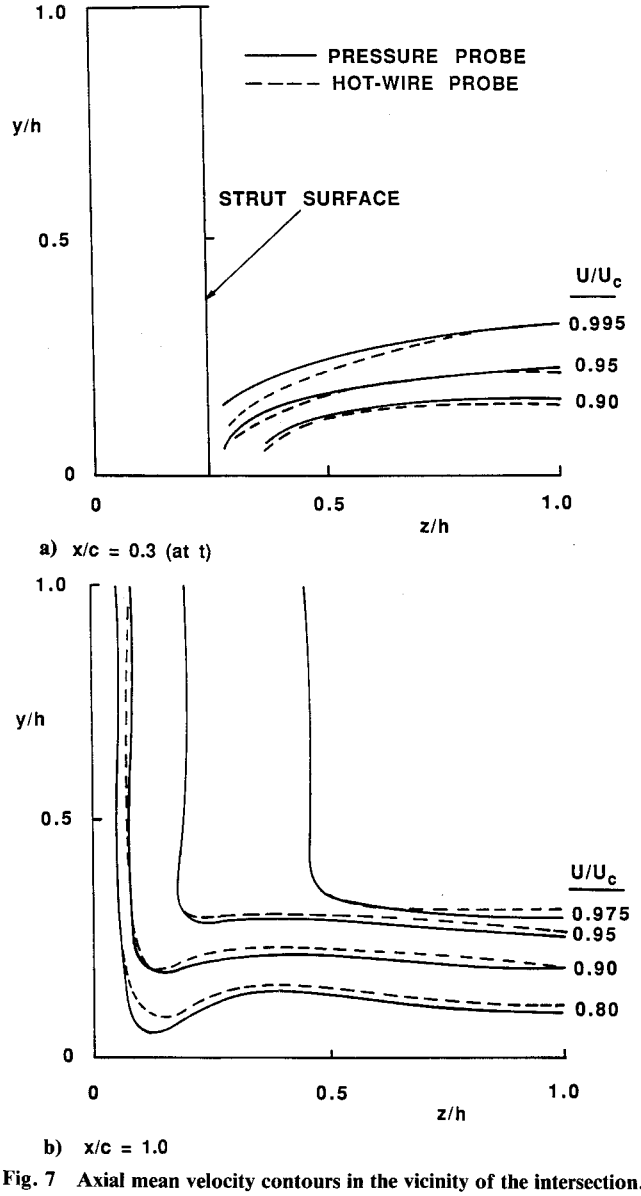

Fig. 7 Axial mean velocity contours in the vicinity of the intersection.

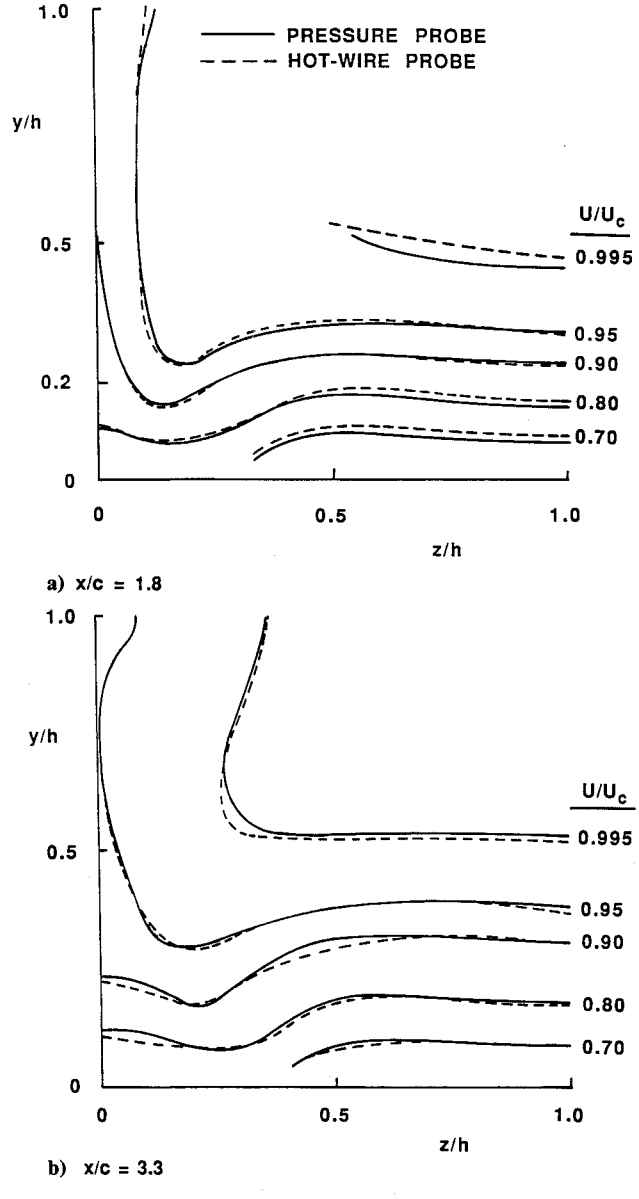

Fig. 8 Axial mean velocity contours in the wake-endwall region.

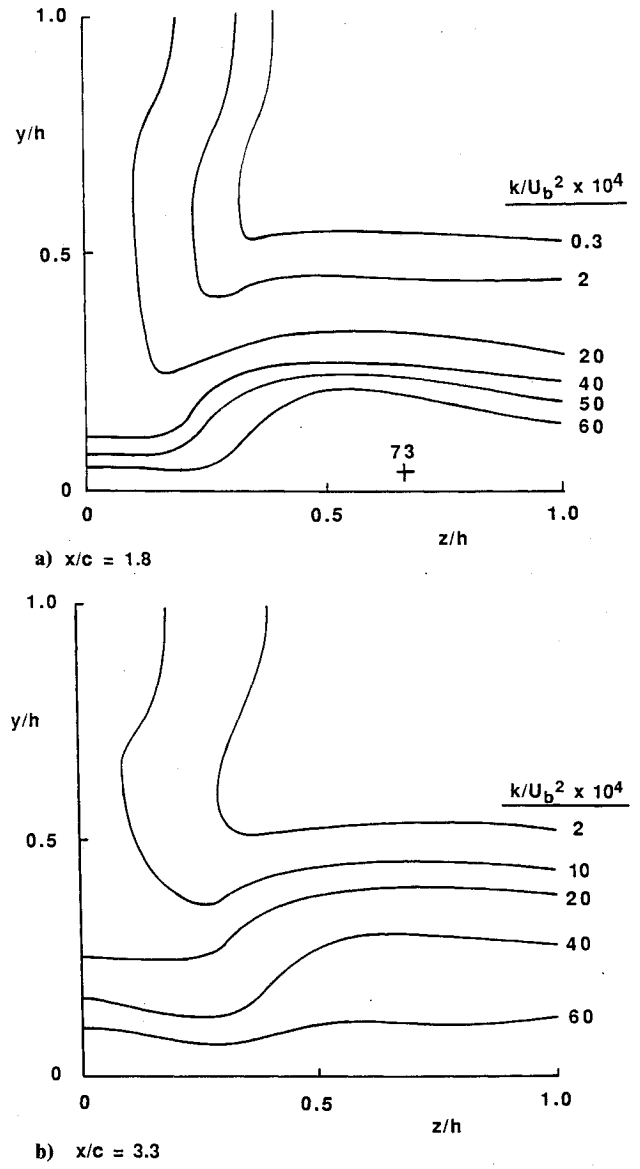

Fig. 9 Turbulence kinetic energy contours in the wake-endwall region.

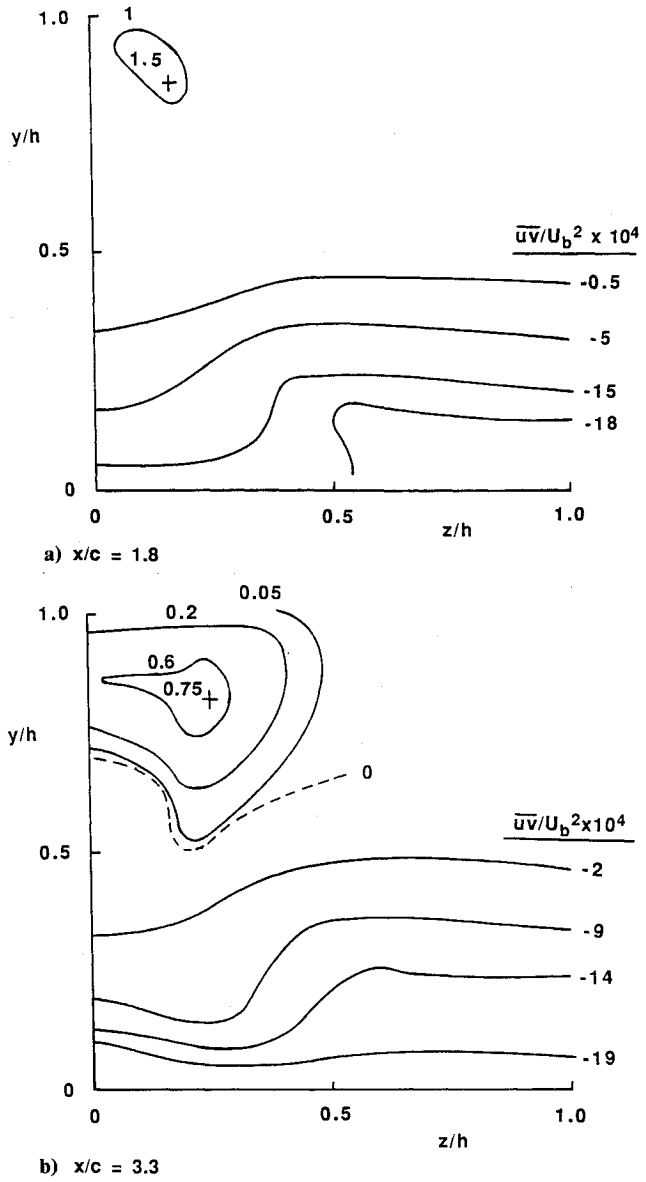

Fig. 10 Reynolds shear stress ($\overline{uv}$) contours in the wake-endwall region.

strut surface, it can be inferred that the secondary vortex is not yet well developed at the strut trailing edge. In the wake-endwall region downstream, however, Fig. 8 shows that the secondary vortex is effective in distorting the primary flow. The level of distortion in the vicinity of the midplane y/h = 1.0, in fact, increases between x/c = 1.8 and 3.3, while distortion induced by the horseshoe vortex near the endwall remains relatively fixed.

Reynolds Stress Results

Turbulence kinetic energy and Reynolds shear stress contours measured in the wake-endwall region are shown in Figs. 9–11. In reference to Fig. 9, it can be seen that turbulence kinetic energy contours in the vicinity of the midplane y/h = 1.0 are distorted by the secondary vortex. The level of distortion is comparable to that induced by the horseshoe vortex near the endwall. A comparison of Figs. 9 and 10 shows that k and $\overline{uv}$ distributions near the endwall are distorted by the horseshoe vortex in a similar manner. This is in accord with anticipated behavior, inasmuch as isocontours of k and $\overline{uv}$ are both initially parallel to the endwall surface upstream of the intersection. Figure 10 shows that isocontours of positive $\overline{uv}$ exist in the vicinity of the midplane y/h = 1.0. This behavior can be explained on the basis of simple eddy viscosity considerations that dictate that $\overline{uv}$ should be positive in regions where $\partial U/\partial y$ is negative, a condition that exists near y/h = 1.0 for the axial mean velocity contours shown in Fig. 8.

The $\overline{uw}$ results in Fig. 11 exhibit more complicated behavior than the results for k and $\overline{uv}$ shown in Figs. 9 and 10. The changes that occur in the sign of this component correlate well with observed changes in the sign of $\partial U/\partial z$. The results shown in Fig. 11a indicate, for example, that along the traverse y/h = 0.2, $\overline{uw}$ is first negative, then positive, and then negative again over the interval $0<z/h<1.0$. At the same streamwise location (x/c = 1.8), Fig. 8a shows that undulations in the axial mean velocity contours are such that $\partial U/\partial z$ is first positive, then negative, and then positive again along this traverse. The condition that the shear stress component be of opposite sign to the axial mean velocity gradient acting in the same plane is not satisfied at all points in the flow, however, as can be seen by referring to Fig. 12. In this figure, shaded regions are shown where $\overline{uv}$ and $\overline{uw}$ have the same sign as $\partial U/\partial y$ and $\partial U/\partial z$, respectively. In these regions, the eddy viscosity is negative, a condition which has also been observed in the vicinity of a wing-body junction[10] and in the wake-endwall region[16] by other investigators. Conventional eddy viscosity models cannot mimic this behavior. The conventional form of the k-ϵ turbulence model is also inadequate for the task, inasmuch as this model employs an eddy viscosity defined as ν_t

$= c_\mu k^2/\epsilon$, where c_μ, k, and ϵ are all positive quantities. Closure at the full Reynolds stress transport equation level may be required, therefore, to predict the present flow with reasonable accuracy.

Near-Wall Behavior

The feasibility of using wall functions to model the endwall flow was examined by analyzing data taken in the near-wall region at $x/c = 3.3$ where the local skewness level was less than 3 deg. Figure 13 shows axial mean velocity contours measured at this location and the corresponding variation in wall shear stress on the endwall. To investigate local law-of-the-wall behavior, axial mean velocity profiles were measured along traverses A through G normal to the endwall, positioned as shown in Fig. 13. The results are shown in Fig. 14 and indicate that local law-of-the-wall behavior exists at each spanwise location, even in the presence of the contour variations that appear in Fig. 13. The conventional forms of the wall functions for k and ϵ, namely $k/U_\tau^2 = 1/\sqrt{c_\mu}$ and $\epsilon y/U_\tau^3 = 1/\kappa$, were also analyzed. The variation of these parameters along two near-wall traverses ($y/h = 0.4$ and 0.12) is shown in Fig. 15, where ϵ was evaluated from the turbulence kinetic energy production rate by assuming local equilibrium. From the figure it can be seen that spanwise variations in the wall functions for k and ϵ diminish as the wall is neared, and that the distributions tend toward the correct limiting values, i.e., $1/\sqrt{c_\mu}$ with $c_\mu = 0.09$ for k/U_τ^2 and $1/\kappa$ with $\kappa = 0.4$ for $\epsilon y/U_\tau^3$. The results shown in Figs. 14 and 15 tend to confirm the validity of applying wall functions to the endwall flow. Caution must be observed, however, inasmuch as the results apply only in the wake-endwall region and not in the immediate vicinity of the intersection, where the distorting influence of the horseshoe

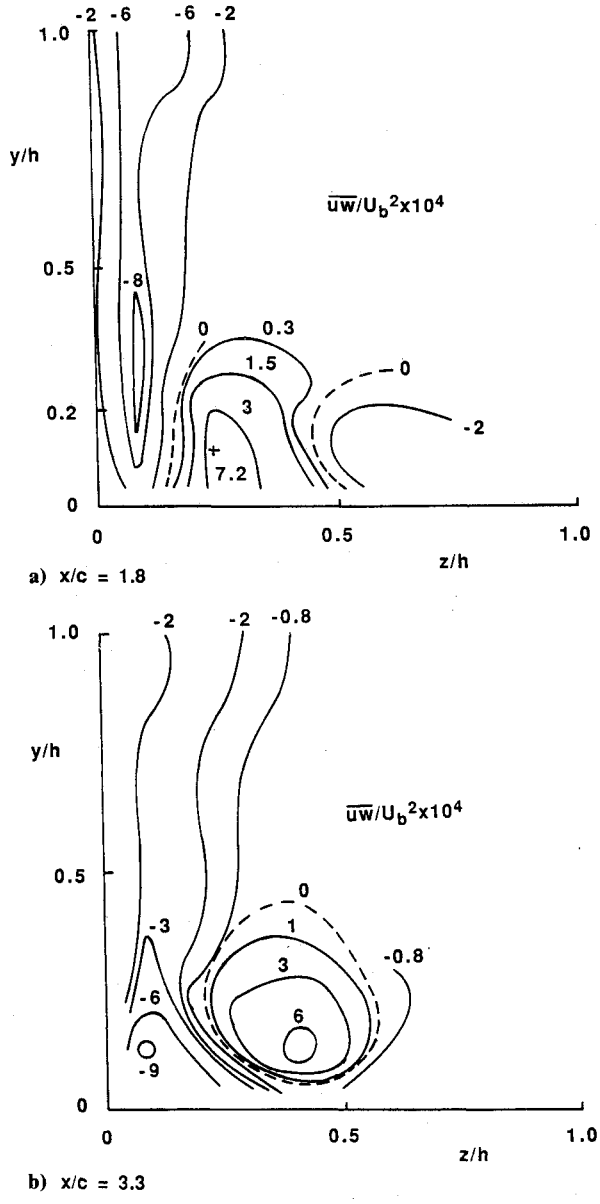

Fig. 11 Reynolds shear stress ($\overline{uw}$) contours in the wake-endwall region.

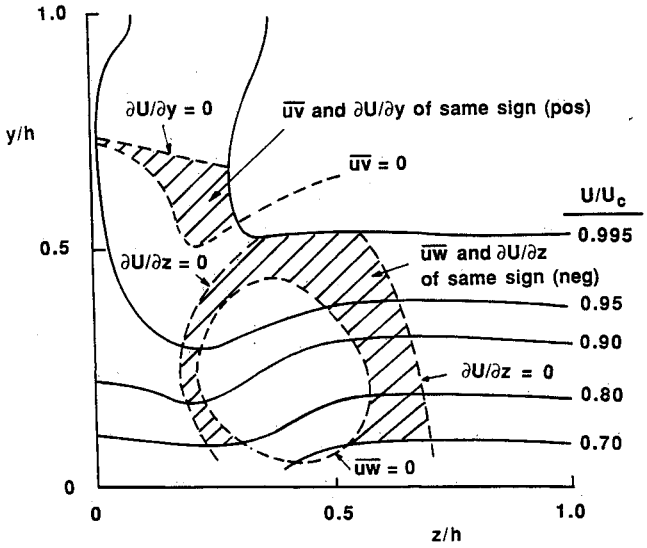

Fig. 12 Regions in the cross plane where $\overline{uv}$ and $\overline{uw}$ are of the same sign as $\partial U/\partial y$ and $\partial U/\partial z$, respectively, at $x/c = 3.3$.

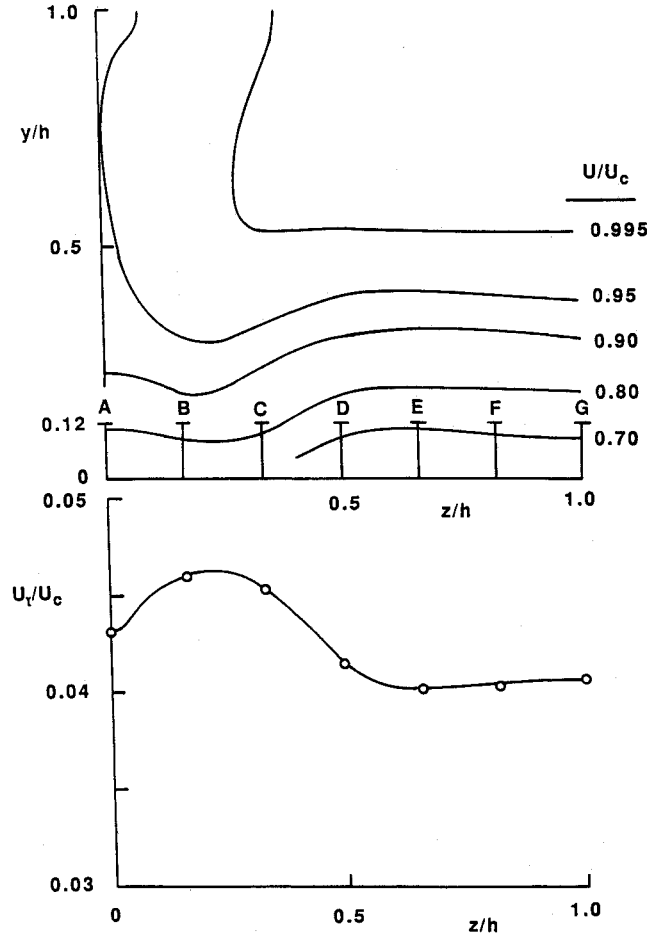

Fig. 13 Axial mean velocity contours and spanwise wall shear stress behavior at $x/c = 3.3$.

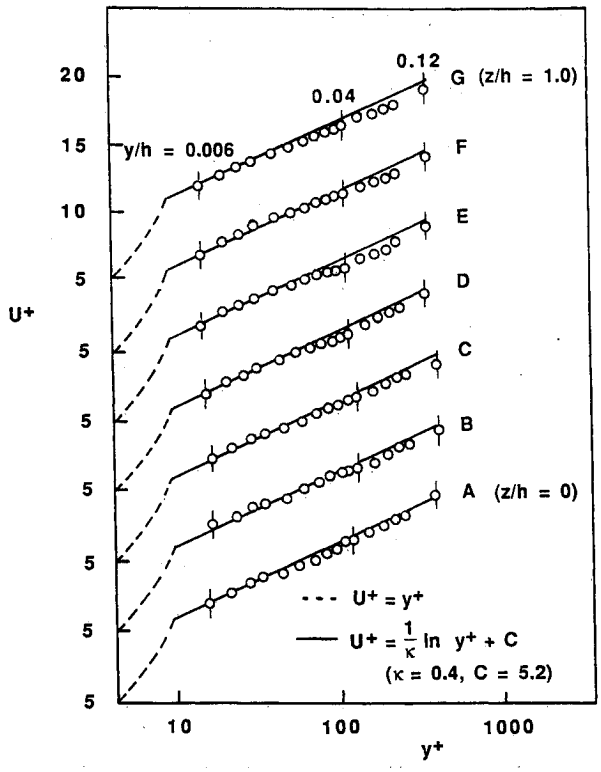

Fig. 14 Law-of-the-wall velocity profiles at different spanwise locations in the near-wall region at $x/c = 3.3$.

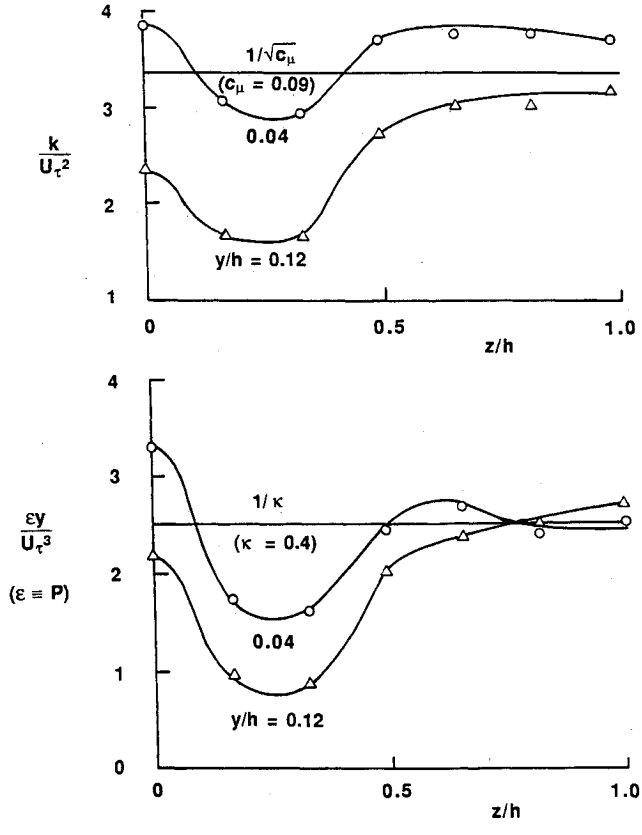

Fig. 15 Turbulence kinetic energy and dissipation rate behavior in the near-wall region at $x/c = 3.3$.

vortex is more pronounced. In this region the local skewness level varies throughout the endwall boundary layer, and the law of the wall may not be applicable when expressed in terms of the mean velocity component parallel to the endwall (the vector sum of U and W) and the resultant wall shear stress on the endwall surface.

Concluding Remarks

Incompressible flow along an unswept NACA 0012 strut bounded by parallel endwalls has been investigated. The endwall boundary layer was tripped upstream of the intersection, but natural transition occurred on the strut surface. For these operating conditions a secondary vortex was formed in addition to the horseshoe vortex generated by endwall flow separation upstream of the strut leading edge. This secondary vortex appears to have been generated as a result of transverse pressure gradients acting on the curved flow between the convex strut surface and duct side wall. The strength of the secondary vortex is approximately the same as that of the horseshoe vortex in the wake-endwall region. Both vortices distort the primary flow and local turbulence structure in this region to the extent that the flow cannot be modeled exactly by means of conventional eddy viscosity or k-ϵ transport equation models. Flow adjacent to the endwall downstream of the intersection appears to be in local equilibrium, so that wall functions can be used for prediction purposes in this region.

Inasmuch as the present flow situation corresponds to flow about a strut-endwall configuration positioned within a constant area duct, the overall flow has to be treated as a confined duct flow problem. In this context, initial conditions for the configuration shown in Fig. 1 are well posed, i.e., $U = U_b$, $V = W = 0$, and $\overline{u^2} = \overline{v^2} = \overline{w^2} = \overline{uv} = \overline{uw} = \overline{vw} = 0$ at the duct inlet. The effect of the boundary-layer trip shown in Fig. 1 can be accommodated by performing the duct flow calculations over a development length that leads to matched conditions with the endwall velocity profiles measured upstream of the strut leading edge at $x/c = -2.0$. As noted earlier, tabulated velocity values at this location are given by Chang.[25] That reference also includes tabulated values for the three mean velocity components and six Reynolds stress components at the four streamwise locations where data were taken ($x/c = 0.3$, 1.0, 1.8, and 3.3). Static pressures measured in the core flow and on the endwall in the vicinity of the intersection are also given by Chang.[25] These results form a fairly complete picture of the changes that occur in the local flow structure on the downstream side of a strut-endwall intersection. Further work will be required to determine the sensitivity of the results to such variables as strut and endwall spacing and to curvature characteristics of the strut surface.

Acknowledgment

This study was supported by the NASA Lewis Research Center under Grant NAG 3-376.

References

[1]Devenport, W. J., and Simpson, R. L., "Turbulence Structure Near the Nose of a Wing-Body Junction," AIAA Paper 87-1310, June 1987.

[2]Devenport, W. J., and Simpson, R. L., "Time-Dependent Structure in Wing-Body Junction Flows," *Turbulent Shear Flows 6*, Springer-Verlag, New York, 1989, pp. 232-248.

[3]Devenport, W. J., and Simpson, R. L., "Time-Dependent and Time-Averaged Turbulence Structure Near the Nose of a Wing-Body Junction", *Journal of Fluid Mechanics*, Vol. 210, Jan. 1990, pp. 23-55.

[4]Baker, C. J., "The Turbulent Horseshoe Vortex," *Journal of Wind Engineering and Industrial Aerodynamics*, Vol. 6, No. 1-2, July 1980, pp. 9-23.

[5]Kornilov, V. I., and Kharitonov, A. M., "Investigation of the Structure of Turbulent Flows in Streamwise Asymmetric Corner Configurations," *Experiments in Fluids*, Vol. 2, No. 4, 1984, pp. 205-212.

[6]Abid, R., and Schmitt, R., "Experimental Study of a Turbulent Horseshoe Vortex Using a Three-Component Laser Velocimeter," AIAA Paper 86-1069, May 1986.

[7]Pierce, F. J., and Tree, I. K., "The Mean Flow Structure on the Symmetry Plane of a Turbulent Junction Vortex," *Journal of Fluids Engineering*, Transactions of the ASME, Vol. 112, March 1990, pp. 16-22.

[8]Devenport, W. L., and Simpson, R. L., "LDV Measurements in the Flow Past a Wing-Body Junction," *Proceedings of the Fourth International Symposium on Applications of Laser Anemometry to Fluid Mechanics*, Lisbon, Portugal, 1988.

[9]Menna, J. D., and Pierce, F. J., "The Mean-Flow Structure Around and Within a Turbulent Junction or Horseshoe Vortex—Part I: The Upstream and Surrounding Three-Dimensional Boundary Layer," *Journal of Fluids Engineering*, Transactions of the ASME, Vol. 110, Dec. 1988, pp. 406–414.

[10]Pierce, F. J., and Harsh, M. D., "The Mean Flow Structure Around and Within a Turbulent Junction or Horseshoe Vortex—Part II. The Separated and Junction Vortex Flow," *Journal of Fluids Engineering*, Transactions of the ASME, Vol. 110, Dec. 1988, pp. 415–423.

[11]Moore J., and Forlini, T. J., "A Horseshoe Vortex in a Duct," *Journal of Engineering for Gas Turbines and Power*, Transactions of the ASME, Vol. 106, No. 3, 1984, pp. 668–676.

[12]Shabaka, I. M. M. A., and Bradshaw, P., "Turbulent Flow Measurements in an Idealized Wing-Body Junction," *AIAA Journal*, Vol. 19, No. 2, Feb. 1981, pp. 131–132.

[13]McMahon, H., Hubbartt, J., and Kubendran, L., "Mean Velocities and Reynolds Stresses in a Juncture Flow," NASA CR-3605, Aug. 1982.

[14]Kubendran, L. R., McMahon, H. M., and Hubbartt, J. E.,"Turbulent Flow Around a Wing/Fuselage-Type Juncture," *AIAA Journal*, Vol. 24, No. 9, 1986, pp. 1447–1452.

[15]Hsing, T-D., and Teng, H-Y., "Experimental Study of the Behavior of 3D-Turbulent Boundary Layer in a Simplified Wing/Body Junction," AIAA Paper 84-1529, June 1984.

[16]Nakayama, A., and Rahai, H. R., "Measurements of Turbulent Flow Behind a Flat Plate Mounted Normal to the Wall," *AIAA Journal*, Vol. 22, No. 12, 1984, pp. 1817–1819.

[17]Özcan, O., and Ölçmen, M. S., "Measurements of Turbulent Flow Behind a Wing-Body Junction," *Proceedings of the Sixth Symposium on Turbulent Shear Flows*, Paul Sabatier Univ., Toulouse, France, Sept. 7-9, 1987, pp. 8-5-1 to 8-5-5.

[18]Özcan, O., and Ölçmen, M. S., "Measurements of Turbulent Flow Behind a Wing-Body Junction," *AIAA Journal*, Vol. 26, No. 4, 1988, pp. 494–496.

[19]Devenport, W. J., Dewitz, M. B., Agarwal, N. K., Simpson, R. L., and Poddar, K., "Effects of a Fillet on the Flow Past a Wing Body Junction," AIAA Paper 89-0986, March 1989.

[20]Mokhtari, S., and Bradshaw, P., "Longitudinal Vortices in Wind Tunnel Wall Boundary Layers," *Aeronautical Journal*, Vol. 87, June/July 1983, pp. 233–236.

[21] Head, M. R., and Vasanta Ram, V., "Simplified Presentation of Preston-Tube Calibration," *The Aeronautical Quarterly*, Vol. 22, Pt. 3, 1971, pp. 295–300.

[22]Gessner, F. B., and Arterberry, S. H., "A Method of Flow Field Determination for Moderately Skewed, Three-Dimensional Flows," *Proceedings of the IUTAM Symposium on Three-Dimensional Turbulent Boundary Layers*, Springer-Verlag, New York, 1982, pp. 79–93.

[23]Po, J. K., "Developing Turbulent Flow in the Entrance Region of a Square Duct," M.S. Thesis, Dept. of Mechanical Engineering, Univ. of Washington, Seattle, WA, 1975.

[24]Arterberry, S. H., "An Improved Method of Flow Field Determination in Three-Dimensional Flows of Low Intensity and Moderate Skewness," M.S. Thesis, Dept. of Mechanical Engineering, Univ. of Washington, Seattle, WA, 1982.

[25]Chang, P. S., "Experimental Investigation of Turbulent Flow Around a Strut-Endwall Configuration," Ph.D. Thesis, Dept. of Mechanical Engineering, Univ. of Washington, Seattle, WA, 1988.

[26]Shabaka, I. M. M. A., "Turbulent Flow in an Idealized Wing-Body Junction," Ph.D. Thesis, Dept. of Aeronautics, Imperial College of Science and Technology, London, 1979.

[27]Mehta, R. D., "Effect of Wing Nose Shape on the Flow in a Wing/Body Junction," *Aeronautical Journal*, Vol. 88, Dec. 1984, pp. 40.

[28]Dickenson, S. C., "Time Dependent Flow Visualization in the Separated Region of an Appendage-Flat Plate Junction," *Experiments in Fluids*, Vol. 6, No. 2, 1988, pp. 140–143.

[29]Harsh, M. D., and Pierce, F. J., "An Experimental Investigation of a Turbulent Junction Vortex," NASA CR-175915, Feb. 1985.

[30]Bradshaw, P., "Turbulent Secondary Flows," *Annual Review of Fluid Mechanics*, Vol. 19, Annual Reviews, Inc., Palo Alto, CA, 1987, pp. 53–74.

[31]Klebanoff, P. S., "Characteristics of Turbulence in a Boundary Layer with Zero Pressure Gradient," NACA Rept. 1247, 1955; also NACA TN 3178, July 1954.